NANO LETTERS

Letter

pubs.acs.org/NanoLett

Condensation of Excitons in a Trap

A. A. High,*[,†] J. R. Leonard,[†] M. Remeika,[†] L. V. Butov,[†] M. Hanson,[‡] and A. C. Gossard[‡]

[†]Department of Physics, University of California at San Diego, La Jolla, California 92093-0319, United States

[‡]Materials Department, University of California at Santa Barbara, Santa Barbara, California 93106-5050, United States

Supporting Information

ABSTRACT: Condensation is observed in a gas of indirect excitons confined in an electrostatic trap. Imaging and interferometric measurements detect that excitons condense at the trap bottom and exciton spontaneous coherence emerges with lowering temperature. Below a temperature of about 1 K, the direct signature of Bose−Einstein condensation, the extension of coherence over the entire cloud, is observed.

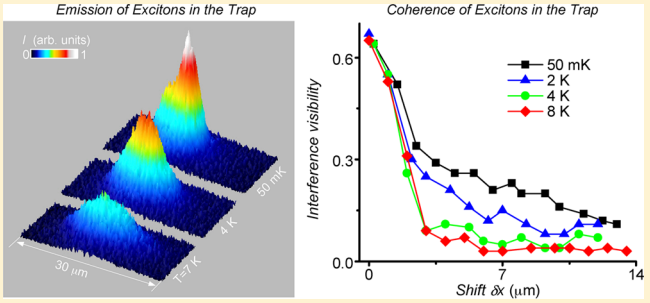

KEYWORDS: *Excitons, traps, coherence, condensation*

The confinement of atomic vapors in traps has led to the realization of Bose−Einstein condensation of atoms.[1−3] Condensation is equivalent to the emergence of spontaneous coherence of matter waves.[4] The detection of spontaneous coherence is a direct experimental measurement of condensation. Here, we report on the observation of condensation and spontaneous coherence in a gas of indirect excitons confined in an electrostatic trap. An exciton is a bound pair of an electron and a hole in a semiconductor. The bosonic nature of excitons allows for their condensation at low temperatures.[5]

Because of recombination excitons have a finite lifetime that is too short to allow cooling to low temperatures in regular semiconductors.[6,7] In order to create a cold exciton gas, the exciton lifetime should be large compared to the exciton cooling time so excitons can cool down to the temperature of the crystal lattice. Furthermore, the realization of a cold and dense exciton gas requires an excitonic state to be the ground state.[8]

These requirements can be fulfilled in a gas of indirect excitons. An indirect exciton is a bound state of an electron and a hole in separate layers (Figure 1a). The spatial separation allows one to control the overlap of electron and hole wave functions and engineer structures with lifetimes of indirect excitons orders of magnitude longer than those of regular excitons.[9,10] In our experiments, indirect excitons are created in a GaAs/AlGaAs coupled quantum well structure (CQW). Long lifetimes of the indirect excitons allow them to cool to low temperatures within about 0.1 K of the lattice temperature, which can be lowered to about 50 mK in an optical dilution refrigerator.[11] This allows the realization of a cold exciton gas with temperature well below the temperature of quantum degeneracy $T_{dB} = 2\pi\hbar^2 n/m$ (for the studied CQW with the exciton mass $m = 0.22m_0$, $T_{dB} \approx 3$ K for the density per spin state $n = 10^{10}$ cm^{-2}).

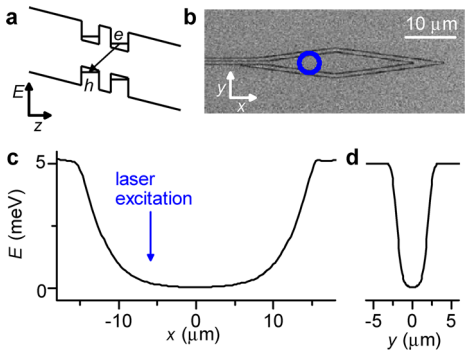

Figure 1. (a) Energy-band diagram of the CQW structure. e, electron; h, hole. (b) SEM image of electrodes forming the diamond trap: a diamond-shaped electrode is surrounded by a thin wire electrode followed by an outer plane electrode. (c,d) Simulation of exciton energy profile through the trap center along x (c) and y (d) for $V_{diamond} = -2.5$ V, $V_{wire} = -2$ V, and $V_{plane} = -2$ V. The position of the laser excitation spot is indicated by the circle in (b) and by the arrow in (c).

Indirect excitons have a built-in dipole moment ed, where d is close to the distance between the QW centers. This allows control of the exciton energy by applied gate voltage; an electric field F_z perpendicular to the QW plane results in the exciton energy shift $E = edF_z$ giving an opportunity to create in-plane potential landscapes for excitons $E(x,y) = edF_z(x,y)$. Advantages of electrostatically created potential landscapes include the opportunity to realize a desired potential profile and control it in situ on a time scale shorter than the exciton lifetime. Excitons

Received: March 10, 2012
Revised: April 9, 2012
Published: April 17, 2012

were studied in various electrostatically created potential landscapes including ramps,[12,13] lattices,[14,15] circuit devices,[16] and traps.[17−23]

Along with electrostatic traps excitons were studied in a variety of traps including strain-induced traps,[24−27] traps created by laser-induced interdiffusion,[28] magnetic traps,[29] and laser-induced traps.[30,31] However, despite intensive studies, no emergence of spontaneous coherence of excitons in a trap was observed until present. Spontaneous coherence of excitons was probed in a ring-shaped trap,[20] however, no enhancement of the interference contrast, and, in turn, the degree of first-order coherence with lowering temperature was shown. Spontaneous coherence of excitons was also probed in a different system, an exciton ring.[32,33] The ring forms on the interface between the electron-rich and hole-rich regions and lacks the crucial advantage of traps which is the opportunity to control the condensates.

Here, we realize an electrostatic trap for indirect excitons using a diamond-shaped electrode (Figure 1b). Because a thinner electrode produces a smaller F_z due to field divergence near the electrode edges, the diamond trap creates a confining potential with the exciton energy gradually reducing toward the trap center (Figure 1c,d).[22] Details are presented in Supporting Information.

The excitons are photoexcited by a 633 nm HeNe laser. The excitation beam is focused to a spot about 5 μm in diameter on a side of the trap (Figure 1b,c). This excitation scheme allows further cooling of the photoexcited excitons when they travel toward the trap center, thus facilitating the realization of a cold exciton gas in the trap (cooling of excitons away from the laser excitation spot also leads to the realization of a cold exciton gas in the inner ring in exciton emission pattern and in laser-induced traps[30]).

The first-order coherence function $g_1(\delta x)$ is measured by shift-interferometry: the emission images produced by arm 1 and 2 of the Mach−Zehnder interferometer (Figure 2a) are

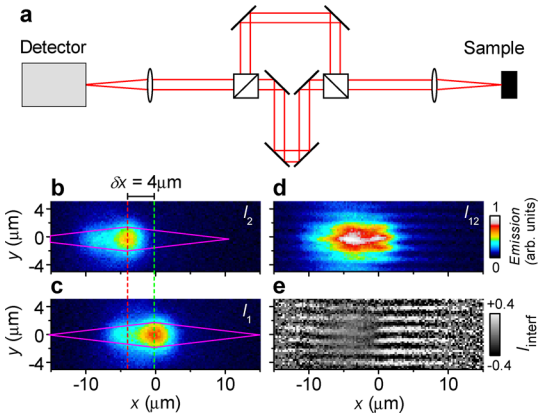

Figure 2. (a) Schematic of the interferometric setup. (b−d) Emission image of indirect excitons measured with arm 2 open (b), arm 1 open (c), and both arms open (d). T_{bath} = 0.1 K, P_{ex} = 1.9 μW. (e) I_{interf} obtained from (b−d).

shifted with respect to each other to measure the interference between the emission of indirect excitons spatially separated by δx. We measure emission intensity I_1 for arm 1 open, I_2 for arm 2 open, and I_{12} for both arms open, and calculate $I_{interf} = [I_{12} - I_1 - I_2]/[2(I_1I_2)^{1/2}]$ (Figure 2b−e). $g_1(\delta x)$ is given by the amplitude of the interference fringes in I_{interf}, see Supporting Information for details.

Figure 3 presents the temperature dependence of exciton emission and interference patterns. At high temperatures, the exciton cloud spreads over the trap resulting in a broad spatial profile of the exciton emission. With lowering temperature, excitons collect at the trap center (Figure 3a,b,c,e). Studies of atoms in traps also show the collection of atoms at the trap center with lowering temperature due to the reduction of the thermal spreading of atoms over the trap and, eventually, condensation of atoms.[1−3]

To determine if condensation of excitons is realized in the trap, we performed shift-interferometry measurements. We found that the exciton collection at the trap center with lowering temperature is accompanied by a strong enhancement of the amplitude of the interference fringes A_{interf} for the interference between the emission of indirect excitons spatially separated by δx (Figure 3d,e). Quantitative characteristics of spontaneous coherence and condensation can be obtained from the measurements of A_{interf} as a function of δx.[4] Such measurements are presented below.

Figure 4a presents $A_{interf}(\delta x)$ for different densities. The exciton temperature is higher in the excitation spot.[30] This is consistent with low values of A_{interf} at negative δx, which correspond to the interference between the emission of a hot exciton gas in the excitation spot and exciton gas in the trap center. We consider positive δx, which correspond to the interference between the emission of an exciton gas in the trap center and exciton gas at positive x further away from the hot excitation spot.

Figure 4c presents the density dependence of the width of the exciton emission pattern along x. At high temperature T_{bath} = 4.5 K, the width of the emission pattern of the exciton cloud monotonically increases with density. This is consistent with screening of the potential landscape in the trap by indirect excitons due to the repulsive exciton−exciton interaction.[22] However, a drastically different behavior is observed at low temperature T_{bath} = 50 mK: the increase of density leads to the reduction of the cloud width, indicating the exciton collection at the trap center. Only at the highest densities, the high-temperature behavior is recovered.

Figure 4b presents the density dependence of A_{interf}. At high temperature T_{bath} = 4.5 K, the coherence degree is low for all densities. However, at low temperature T_{bath} = 50 mK, the increase of density leads to a strong enhancement of A_{interf}, followed by its reduction. As in the case of varying temperature (Figure 3e), with varying density, the exciton collection at the trap center is accompanied by the enhancement of the coherence degree of excitons (Figure 4b,c).

The density at which the coherence degree of excitons is close to maximum (Figure 4b) has been chosen to study the temperature dependence due to the strongest coherence enhancement with reducing temperature. Figure 5a presents the amplitude of the interference fringes $A_{interf}(\delta x)$ for different temperatures. The spatial extension of $A_{interf}(\delta x)$ can be characterized by a coherence length ξ at which the interference visibility drops e times. A strong enhancement of the exciton coherence length is observed at low temperatures (Figure 5c). While at high temperatures ξ is considerably smaller than the exciton cloud width, at low temperatures the entire exciton cloud becomes coherent (Figures 3e, 5).

The data are discussed below. In the reported experiments, the laser excitation energy exceeds the exciton energy by about

dx.doi.org/10.1021/nl300983n | Nano Lett. 2012, 12, 2605−2609

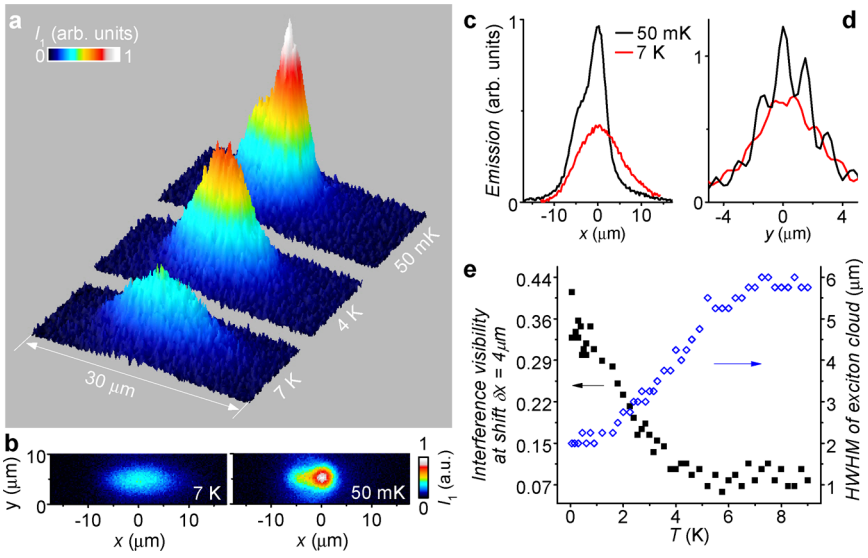

Figure 3. (a,b) Emission patterns I_1 for temperatures T_{bath} = 7, 4, and 0.05 K. (c,d) Spatial profiles of the emission patterns (c) and interference patterns I_{12} at shift δx = 4 μm (d) for T_{bath} = 7 K (red) and 0.05 K (black). (e) Amplitude of the interference fringes A_{interf} at shift δx = 4 μm averaged over 0 < x < 1.5 μm (black squares) and half-width at half-maximum (hwhm) of the exciton emission pattern along x (blue diamonds) vs temperature. P_{ex} = 1.9 μW.

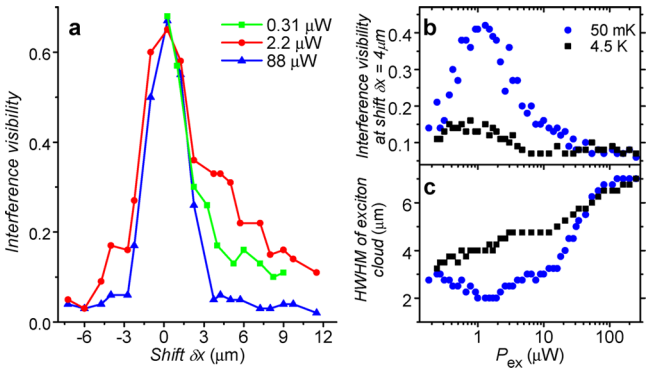

Figure 4. (a) Amplitude of the interference fringes $A_{interf}(\delta x)$ for excitons in the trap for excitation density P_{ex} = 0.31 μW (green squares), 2.2 μW (red circles), and 88 μW (blue triangles) at T_{bath} = 50 mK. (b,c) A_{interf} at shift δx = 4 μm averaged over 0 < x < 1.5 μm (b) and hwhm of the exciton emission pattern along x (c) vs P_{ex} for T_{bath} = 50 mK (blue circles) and 4.5 K (black squares).

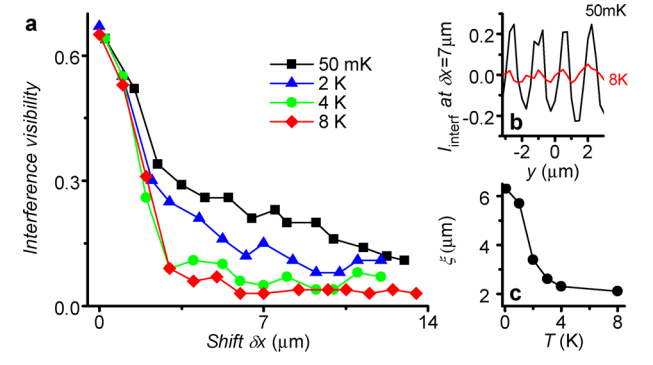

Figure 5. (a) $A_{interf}(\delta x)$ for excitons in the trap for T_{bath} = 50 mK (black squares), 2 K (blue triangles), 4 K (green circles), and 8 K (red diamonds). (b) I_{interf} for T_{bath} = 50 mK (black) and 8 K (red) at shift δx = 7 μm. (c) The exciton coherence length ξ as a function of temperature. P_{ex} = 1.9 μW.

400 meV and the laser excitation spot is spatially separated from the interfering excitons for positive δx. Therefore studied coherence in the exciton gas is spontaneous coherence; it is not induced by coherence of the laser excitation. (Note that for negative δx, the interfering excitons spatially overlap with the laser excitation spot and exciton coherence is suppressed (Figure 4a), confirming that exciton coherence is not induced by the laser excitation.)

The coherence of an exciton gas is imprinted on the coherence of emission, which is described by the first-order coherence function $g_1(\delta x)$. In turn, this function is given by the amplitude of the interference fringes $A_{interf}(\delta x)$ in "the ideal experiment" with perfect spatial resolution. In real experiments, the measured $A_{interf}(\delta x)$ is given by the convolution of $g_1(\delta x)$ with the point-spread function (PSF) of the optical system used in the experiment.[33] The PSF is determined by measuring the emission profile across a source of vanishing width, see Supporting Information. The PSF is a peak at δx = 0 of the width corresponding to the spatial resolution of the optical system. A peak in $A_{interf}(\delta x)$ at δx = 0 due to the PSF can be seen both at low and high temperatures.

Both for a classical gas and quantum gas $g_1(\delta x)$ is close to 1 at δx = 0 and drops with increasing δx within the coherence length ξ. The difference between the classical and quantum gas is in the value of ξ. For a classical gas, ξ_{cl} is close to the thermal de Broglie wavelength $\lambda_{dB} = (2\pi\hbar^2/mT)^{1/2}$, which is well below the PSF width in the studied temperature range ($\xi_{cl} < \xi_{cl@0.1K} \sim$ 0.5 μm, the PSF width is ~2 μm). Therefore, for a classical gas at temperatures above 4 K, the measured ξ is given by the PSF width (Figure 5).

For a classical gas, the coherence length $\xi \propto T^{-1/2}$ gradually increases with reducing temperature and remains small <0.5 μm for T > 0.1 K, much smaller than the coherence length observed at the lowest temperatures (Figure 5). Therefore, an increase of the coherence length in a classical gas cannot lead to the increase in the contrast of the interference pattern at large δx observed in the experiment (Figure 5).

In contrast, for a condensate the coherence length becomes much larger than the thermal de Broglie wavelength and

dx.doi.org/10.1021/nl300983n | Nano Lett. 2012, 12, 2605−2609

reaches the size of the exciton cloud in the trap so the entire exciton cloud becomes coherent. This signature of Bose–Einstein condensation is observed at the lowest temperatures in the experiment (Figures 3e, 5). The measured transition temperature is ~2 K (Figure 5c). Estimates of the temperature of exciton BEC in the trap are close to 2 K, see Supporting Information.

Finally, Figure 5a also illustrates why δx = 4 μm is selected for presenting coherence degree of excitons in Figures 3 and 4. The shift δx = 4 μm exceeds both λ_{dB} and the PSF width. At such δx, only weak coherence given by the PSF value at δx = 4 μm can be observed for a classical gas. Higher A_{interf} exceeding such background level reveal spontaneous coherence of excitons.

The realization of exciton condensate in a trap opens the opportunity to study the condensate properties. Traps allow precise control of condensates by in situ control of trap shape and depth that has been effectively used in studies of condensates of atoms. Similar control of condensates of excitons in condensed matter materials will allow studying condensates with parameters, such as mass, interaction, temperature, and characteristic times, orders of magnitude different from those in condensates of atoms. This will be the subject for future research.

■ ASSOCIATED CONTENT

Supporting Information

In Supporting Information we present the following: sample structure; details of shift-interferometry measurements and analysis; emission spectra and Fourier spectroscopy measurements; measurement of the point spread function; and estimates of the temperature of Bose–Einstein condensation of excitons in the trap. This material is available free of charge via the Internet at http://pubs.acs.org.

■ AUTHOR INFORMATION

Corresponding Author

*E-mail: alex.high@gmail.com.

Notes

The authors declare no competing financial interest.

■ ACKNOWLEDGMENTS

We thank Michael Fogler for discussions. This work was supported by ARO Grant W911NF-08-1-0341 and NSF Grant 0907349. The development of spectroscopy in a dilution refrigerator was also supported by the DOE award DE-FG02-07ER46449.

■ REFERENCES

(1) Anderson, M. H.; Ensher, J. R.; Matthews, M. R.; Wieman, C. E.; Cornell, E. A. Observation of Bose–Einstein condensation in a dilute atomic vapor. *Science* **1995**, *269*, 198–201.

(2) Bradley, C. C.; Sackett, C. A.; Tollett, J. J.; Hulet, R. G. Evidence of Bose–Einstein condensation in an atomic gas with attractive interactions. *Phys. Rev. Lett.* **1995**, *75*, 1687–1690.

(3) Davis, K. B.; Mewes, M.-O.; Andrews, M. R.; van Druten, N. J.; Durfee, D. S.; Kurn, D. M.; Ketterle, W. Bose–Einstein condensation in a gas of sodium atoms. *Phys. Rev. Lett.* **1995**, *75*, 3969–3973.

(4) Penrose, O.; Onsager, L. Bose–Einstein Condensation and Liquid Helium. *Phys. Rev.* **1956**, *104*, 576–584.

(5) Keldysh, L. V.; Kozlov, A. N. Collective Properties of Excitons in Semiconductors. *Sov. Phys. JETP* **1968**, *27*, 521–528.

(6) Tikhodeev, S. G.; Kopelevich, G. A.; Gippius, N. A. Exciton transport in Cu_2O: phonon wind versus superfluidity. *Phys. Status Solidi B* **1998**, *206*, 45–53.

(7) Jang, J. I.; Wolfe, J. P. Auger recombination and biexcitons in Cu_2O: A case for dark excitonic matter. *Phys. Rev. B* **2006**, *74*, 045211.

(8) Keldysh, L. V. The electron-hole liquid in semiconductors. *Contemp. Phys.* **1986**, *27*, 395–428.

(9) Lozovik, Y. E.; Yudson, V. I. New mechanism for superconductivity: pairing between spatially separated electrons and holes. *Sov. Phys. JETP* **1976**, *44*, 389–397.

(10) Fukuzawa, T.; Kano, S. S.; Gustafson, T. K.; Ogawa, T. Possibility of coherent light emission from Bose condensed states of SEHPs. *Surf. Sci.* **1990**, *228*, 482–485.

(11) Butov, L. V.; Ivanov, A. L.; Imamoglu, A.; Littlewood, P. B.; Shashkin, A. A.; Dolgopolov, V. T.; Campman, K. L.; Gossard, A. C. Stimulated scattering of indirect excitons in coupled quantum wells: Signature of a degenerate Bose-gas of excitons. *Phys. Rev. Lett.* **2001**, *86*, 5608–5611.

(12) Hagn, M.; Zrenner, A.; Böhm, G.; Weimann, G. Electric-field-induced exciton transport in coupled quantum well structures. *Appl. Phys. Lett.* **1995**, *67*, 232–235.

(13) Gärtner, A.; Holleitner, A. W.; Kotthaus, J. P.; Schuh, D. Drift mobility of long-living excitons in coupled GaAs quantum wells. *Appl. Phys. Lett.* **2006**, *89*, 052108.

(14) Zimmermann, S.; Schedelbeck, G.; Govorov, A. O.; Wixforth, A.; Kotthaus, J. P.; Bichler, M.; Wegscheider, W.; Abstreiter, G. Spatially resolved exciton trapping in a voltage-controlled lateral superlattice. *Appl. Phys. Lett.* **1998**, *73*, 154–156.

(15) Remeika, M.; Graves, J. C.; Hammack, A. T.; Meyertholen, A. D.; Fogler, M. M.; Butov, L. V.; Hanson, M.; Gossard, A. C. Localization-delocalization transition of indirect excitons in lateral electrostatic lattices. *Phys. Rev. Lett.* **2009**, *102*, 186803.

(16) High, A. A.; Novitskaya, E. E.; Butov, L. V.; Hanson, M.; Gossard, A. C. Control of exciton fluxes in an excitonic integrated circuit. *Science* **2008**, *321*, 229–231.

(17) Huber, T.; Zrenner, A.; Wegscheider, W.; Bichler, M. Electrostatic exciton traps. *Phys. Status Solidi A* **1998**, *166*, R5–R6.

(18) Hammack, A. T.; Gippius, N. A.; Sen, Y.; Andreev, G. O.; Butov, L. V.; Hanson, M.; Gossard, A. C. Excitons in electrostatic traps. *J. Appl. Phys.* **2006**, *99*, 066104.

(19) Chen, G.; Rapaport, R.; Pfeifer, L. N.; West, K.; Platzman, P. M.; Simon, S.; Vörös, Z.; Snoke, D. Artificial trapping of a stable high-density dipolar exciton fluid. *Phys. Rev. B* **2006**, *74*, 045309.

(20) Gorbunov, A. V.; Timofeev, V. B. Large-scale coherence of the Bose condensate of spatially indirect excitons. *JETP Lett.* **2006**, *84*, 329–334.

(21) High, A. A.; Hammack, A. T.; Butov, L. V.; Mouchliadis, L.; Ivanov, A. L.; Hanson, M.; Gossard, A. C. Indirect Excitons in Elevated Traps. *Nano Lett.* **2009**, *9*, 2094–2098.

(22) High, A. A.; Thomas, A. K.; Grosso, G.; Remeika, M.; Hammack, A. T.; Meyertholen, A. D.; Fogler, M. M.; Butov, L. V.; Hanson, M.; Gossard, A. C. Trapping indirect excitons in a GaAs quantum-well structure with a diamond-shaped electrostatic trap. *Phys. Rev. Lett.* **2009**, *103*, 087403.

(23) Schinner, G. J.; Schubert, E.; Stallhofer, M. P.; Kotthaus, J. P.; Schuh, D.; Rai, A. K.; Reuter, D.; Wieck, A. D.; Govorov, A. O. Electrostatically trapping indirect excitons in coupled $In_xGa_{1-x}As$ quantum wells. *Phys. Rev. B* **2011**, *83*, 165308.

(24) Trauernicht, D. P.; Mysyrowicz, A.; Wolfe, J. P. Strain confinement and thermodynamics of free excitons in a direct-gap semiconductor. *Phys. Rev. B* **1983**, *28*, 3590–3592.

(25) Kash, K.; Worlock, J. M.; Sturge, M. D.; Grabbe, P.; Harbison, J. P.; Scherer, A.; Lin, P. S. D. Strain-induced lateral confinement of excitons in GaAs/AlGaAs quantum well microstructures. *Appl. Phys. Lett.* **1988**, *53*, 782–784.

(26) Naka, N.; Nagasawa, N. Bosonic stimulation of cold excitons in a harmonic potential trap in Cu_2O. *J. Lumin.* **2005**, *112*, 11–16.

(27) Yoshioka, K.; Chae, E.; Kuwata-Gonokami, M. Transition to a Bose−Einstein condensate and relaxation explosion of excitons at sub-Kelvin temperatures. *Nat. Commun.* **2011**, *2*, 328.
(28) Brunner, K.; Bockelmann, U.; Abstreiter, G.; Walther, M.; Böhm, G.; Tränkle, G.; Weimann, G. Photoluminescence from a single GaAs/AlGaAs quantum dot. *Phys. Rev. Lett.* **1992**, *69*, 3216−3219.
(29) Christianen, P. C. M.; Piazza, F.; Lok, J. G. S.; Maan, J. C.; van der Vleuten, W. Magnetic trap for excitons. *Physica B* **1998**, *249*, 624−627.
(30) Hammack, A. T.; Griswold, M.; Butov, L. V.; Smallwood, L. E.; Ivanov, A. L.; Gossard, A. C. Trapping of cold excitons in quantum well structures with laser light. *Phys. Rev. Lett.* **2006**, *96*, 227402.
(31) Alloing, M.; Lemaître, A.; Galopin, E.; Dubin, F. On-demand confinement of semiconductor excitons by all-optical control. arXiv:1202.3301v1.
(32) Sen, Y.; Hammack, A. T.; Fogler, M. M.; Butov, L. V.; Gossard, A. C. Coherence Length of Cold Exciton Gases in Coupled Quantum Wells. *Phys. Rev. Lett.* **2006**, *97*, 187402.
(33) Fogler, M. M.; Sen, Y.; Hammack, A. T.; Butov, L. V.; Gossard, A. C. Effect of spatial resolution on the estimates of the coherence length of excitons in quantum wells. *Phys. Rev. B* **2008**, *78*, 035411.

Supporting information for "Condensation of excitons in a trap"

A.A. High,[1] J.R. Leonard,[1] M. Remeika,[1] L.V. Butov,[1] M. Hanson,[2] and A.C. Gossard[2]

[1]*Department of Physics, University of California at San Diego, La Jolla, CA 92093-0319, USA*
[2]*Materials Department, University of California at Santa Barbara, Santa Barbara, CA 93106-5050, USA*

(Dated: April 18, 2012)

Structure

The CQW structure is grown by MBE. An n^+-GaAs layer with $n_{Si} = 10^{18}$ cm^{-3} serves as a homogeneous bottom electrode. The top electrodes are fabricated via e-beam lithography by depositing a semitransparent layer of Ti (2 nm) and Pt (8 nm). The device includes a $3.5 \times 30\mu$m diamond electrode, a 600 nm wide 'wire' electrode around the diamond, and 'outer plane' electrode. Two 8 nm GaAs QWs separated by a 4 nm $Al_{0.33}Ga_{0.67}As$ barrier are positioned 100 nm above the n^+-GaAs layer within an undoped 1 μm thick $Al_{0.33}Ga_{0.67}As$ layer. Positioning the CQW closer to the homogeneous electrode suppresses the in-plane electric field [1], which otherwise can lead to exciton dissociation.

Experimental setup. Shift-interferometry measurements.

We use a Mach-Zehnder (MZ) interferometer to probe coherence of indirect excitons (Fig. 2a in the main text). The emission beam is made parallel by an objective inside the optical dilution refrigerator and lenses. In the shift-interferometry measurements, the path lengths of arm 1 and arm 2 are set equal. The interfering emission images produced by arm 1 and 2 of the MZ interferometer are shifted relative to each other along x to measure the interference between the emission of excitons, which are laterally separated by δx. The shift δx is determined from the images produced by arm 1 and arm 2 (Fig. 2b,c in the main text). It is controlled by the interferometer mirrors. The emission is filtered by an interference filter of linewidth ± 5, nm adjusted to the emission wavelength of indirect excitons $\lambda = 800$ nm, see Fig. 1a. The signal is focused to produce an image of emission of indirect excitons. The image is recorded by a liquid-nitrogen cooled CCD. We measure emission intensity I_1 for arm 1 open, I_2 for arm 2 open, and I_{12} for both arms open, and then calculate

$$I_{\rm interf} = (I_{12} - I_1 - I_2)/(2\sqrt{I_1 I_2}\,)\,. \qquad (1)$$

In general, for two partially coherent sources located at $\mathbf{r}_1$ and $\mathbf{r}_2$, one has the relation [2],

$$I_{\rm interf} = \cos\delta\theta(\mathbf{r}_1,\mathbf{r}_2)\,\zeta(\mathbf{r}_1,\mathbf{r}_2)\,, \qquad (2)$$

where $\delta\theta(\mathbf{r}_1,\mathbf{r}_2)$ is the phase difference of the two sources and $\zeta(\mathbf{r}_1,\mathbf{r}_2)$ is their degree of coherence. In our experimental geometry, there is a small tilt angle α between the image planes of the two arms. As a result, the phase difference

$$\delta\theta(\mathbf{r}_1,\mathbf{r}_2) = q_t y + \phi(\mathbf{r}_1,\mathbf{r}_2) \qquad (3)$$

has a component linear in y — the coordinate in the direction perpendicular to the tilt axis — which produces periodic oscillation of $I_{\rm interf}$. The period of the interference fringes is set by $q_t = 2\pi\alpha/\lambda$. The coherence function $\zeta(\mathbf{r}_1,\mathbf{r}_2)$ for $\mathbf{r}_1 - \mathbf{r}_2 = \delta\mathbf{x}$ is given by the amplitude of these interference fringes.

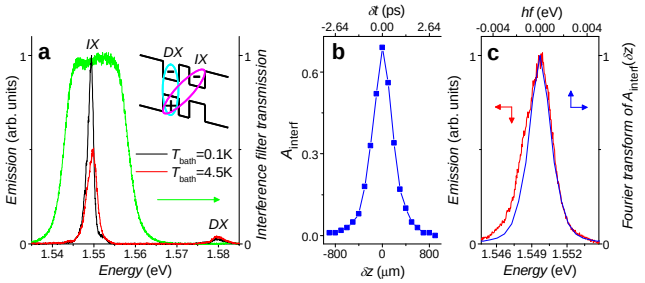

FIG. 1: (**a**) Emission spectra in the center of the trap for $T_{bath} = 0.1$ K (black line) and 4.5 K (red line) measured by spectrometer. Emission of direct excitons (DX) and indirect excitons (IX) is indicated. Green line presents the transmission curve of the interference filter used in the shift-interferometry, Fourier-spectroscopy, and imaging experiments. Inset: band diagram of the CQW with direct and indirect excitons. (**b**) Fourier-spectroscopy measurements: Amplitude of interference fringes $A_{\rm interf}$ vs. the difference in the path lengths of arm 1 and arm 2 of the MZ interferometer δz and corresponding time delay δt for indirect excitons in the center of the trap at $T_{bath} = 4.5$ K. (**c**) Calculated spectrum based on Fourier transform of $A_{\rm interf}(\delta t)$ in (**b**) (blue line) and spectrum of indirect excitons measured by spectrometer in the center of the trap at $T_{bath} = 4.5$ K (red line). $P_{ex} = 1.9\,\mu$W.

Emission spectra. Fourier spectroscopy measurements.

Figure 1a presents the spectra at low and high temperature measured by spectrometer. In all interference and imaging experiments in the paper, only the emission of indirect excitons (IX) is measured. This is achieved by using an interference filter. The transmission curve of the interference filter is presented in Fig. 1a. This curve shows that the contribution of the weak emission of direct excitons (DX) or any other emission (such as

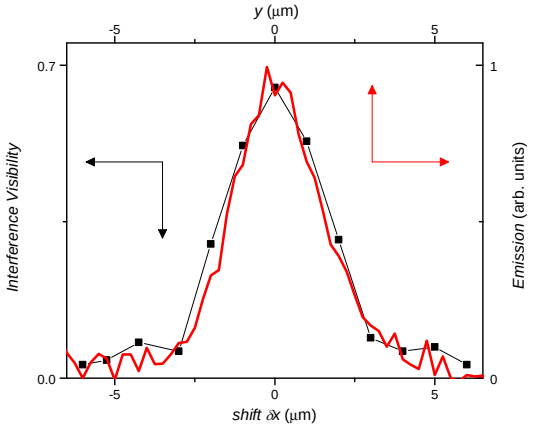

FIG. 2: Interference visibility vs. shift δx for excitons in trap at $T_{bath} = 8$ K (black squares) and y-axis cross section of exciton emission in a segment of the thin wire on the left from the diamond, see Fig. 1b in the main text (red line). The width of the wire, 0.6 μm, is significantly smaller than the spatial resolution and, therefore, the wire can be considered as a source of vanishing width.

low-energy bulk emission) has been cut off by the interference filter. Therefore, any change of the amplitude of the interference fringes $A_{interf}(\delta x)$ and, in turn, the coherence length measured in our experiments is due to a change of coherence of indirect excitons.

We also measured amplitude of interference fringes $A_{\rm interf}$ vs. the difference in the path lengths of arm 1 and arm 2 of the MZ interferometer δz and corresponding time delay δt for indirect excitons in the center of the trap (Fig. 1b). The spectrum obtained by this Fourier-spectroscopy measurement is in a good agreement with the spectrum measured by spectrometer (Fig. 1c).

Measurement of the point-spread function.

The point-spread function (PSF) of the optical setup is measured by exciting a segment of the thin wire on the left from the diamond (see Fig. 1b in the main text) and measuring the spatial profile of exciton emission across the wire (Fig. 2). The width of this wire is 0.6 μm, significantly smaller than the PSF width for our optical setup. Therefore, the wire can be considered as a source of vanishing width so the spatial profile of exciton emission across the wire is given by the PSF. This independent measure of the PSF is in good agreement with the $A_{interf}(\delta x)$ function at high temperatures $T \gtrsim 4$ K (Fig. 5 in the main text) that is given by the PSF width.

Interference images.

In this section, we present examples of interference images and their cross-sections providing technical details to the data presented in the main text of the paper.

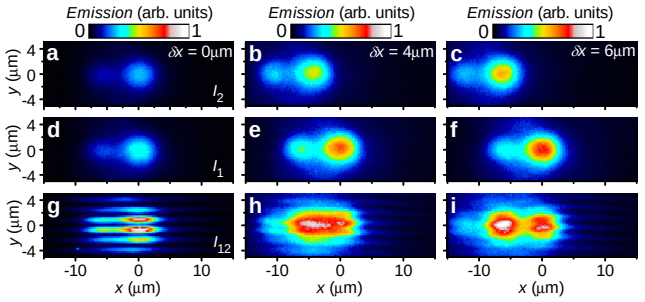

FIG. 3: Emission images I_2 for arm 2 open (a-c), emission images I_1 for arm 1 open (d-f), and interference images I_{12} for both arms open (g-i) for shift $\delta x = 0$ (a,d,g), 4 μm (b,e,h), and 6 μm (c,f,i). $T_{bath} = 0.1$ K, $P_{ex} = 1.9\,\mu$W.

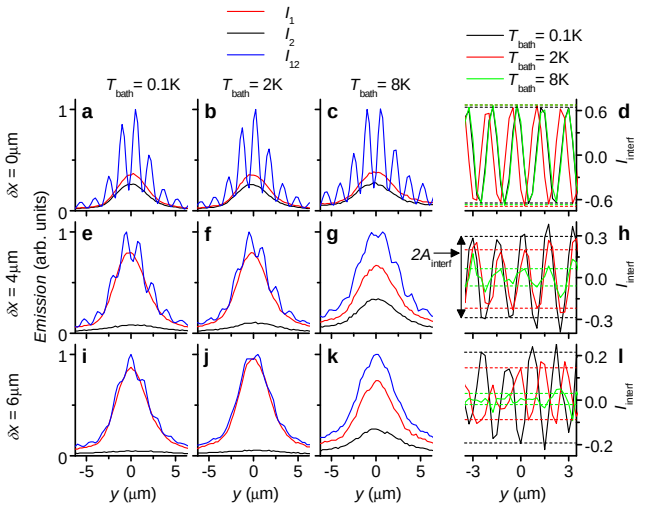

FIG. 4: (a-c, e-g, i-k) Spatial profiles along y at $x = 0$ of I_1 (red), I_2 (black), and I_{12} (blue) at shift $\delta x = 0$ (a-c), 4 μm (e-g), and 6 μm (i-k). $T_{bath} = 0.1$ K (a,e,i), 2 K (b,f,j), and 8 K (c,g,k). (d,h,l) Spatial profiles along y at $x = 0$ of $I_{\rm interf}$ at $T_{bath} = 0.1$ K (black), 2 K (red), and 8 K (green) for $\delta x = 0$ (d), 4 μm (h), and 6 μm (l). Amplitudes of interference fringes A_{intef} are indicated by dashed lines. $P_{ex} = 1.9\mu$W.

Figure 3 presents emission images I_1 for arm 1 open, emission images I_2 for arm 2 open, and interference images I_{12} for both arms open for different shifts δx. Figure 4 presents cross-sections of interference images I_{12} and $I_{\rm interf} = (I_{12} - I_1 - I_2)/(2\sqrt{I_1 I_2}\,)$ for different δx and temperatures.

Transition temperature.

In this section, we estimate the temperature of Bose-Einstein condensation (BEC) of excitons in the trap and compare it with the measured condensation temperature. For a rough estimate, we use the formula for BEC in a system of ideal noninteracting bosons in a parabolic 2D trap [3–5]: $T_c = \frac{\sqrt{6}}{\pi}\hbar\omega_{2D}\sqrt{N/g}$, where $\omega_{2D} = (\omega_x\omega_y)^{1/2}$,

ω_x and ω_y are the trap oscillator frequencies, g is the spin degeneracy, and N is the number of particles in the trap. A parabolic fit to the trap profile (Fig. 1c,d in the main text) $E(x,y) = \frac{m}{2}(\omega_x^2 x^2 + \omega_y^2 y^2)$ gives for $g = 4$ and exciton mass $m = 0.22m_0$ [6]: $\omega_x \sim 4 \times 10^9$ s^{-1}, $\omega_y \sim 3 \times 10^{10}$ s^{-1}, and $T_c \sim 0.03\sqrt{N}$.

The exciton density n can be estimated from the energy shift. For the data in Fig. 5 at the lowest temperatures, the measured energy shift $\delta E \approx 1.3$ meV. Using the plate capacitor formula for the density estimate $\delta E = 4\pi e^2 n d/\varepsilon$ [7–9], where $d \approx 12$ nm is the separation between the electron and hole layers for our sample and ε is the background dielectric constant, gives $n \sim 10^{10}$ cm^{-2}. For the size of the exciton cloud in the trap ~ 10 μm^2 (Fig. 3 in the main text), a total exciton number in the trap $N \sim 10^3$. This gives $T_c \sim 1$ K.

The plate capacitor formula underestimates the density [10, 11]. Using the correction for the relation between δE and n estimated in [12], we obtain from the energy shift $N \sim 3 \times 10^3$ [13] and $T_c \sim 2$ K. These rough estimates of the temperature of exciton BEC in the trap are close to the measured transition temperature ~ 2 K (Fig. 5c in the main text).

[1] Hammack, A.T.; Gippius, N.A.; Sen Yang; Andreev, G.O.; Butov, L.V.; Hanson, M.; Gossard, A.C. Excitons in electrostatic traps. *J. Appl. Phys.* **2006**, 99, 066104

[2] Milonni, P.W.; Eberly, J.H. *Lasers* (Wiley, New York, 1988).

[3] Ketterle, W.; van Druten, N.J. Bose-Einstein condensation of a finite number of particles trapped in one or three dimensions. *Phys. Rev. A* **1996**, 54, 656

[4] Mullin, W.J.; Bose-Einstein Condensation in a Harmonic Potential. *J. Low Temp. Phys.* **1997**, 106, 615

[5] Dalfovo, F; Giorgini, S.; Pitaevskii, L.P.; Stringari, S. Theory of Bose-Einstein condensation in trapped gases. *Rev. Mod. Phys.* **1999**, 71, 463

[6] Butov, L.V.; Mintsev, A.V.; Lozovik, Yu.E.; Campman, K.L.; Gossard. A.C. From spatially indirect excitons to momentum-space indirect excitons by an in-plane magnetic field. *Phys. Rev. B* **2000**, 62, 1548

[7] Yoshioka, D.; MacDonald, A.H. Double Quantum Well Electron-Hole Systems in Strong Magnetic Fields. *J. Phys. Soc. Jpn.* **1990** 59, 4211

[8] Zhu, X; Littlewood, P.B.; Hybertsen, M.; Rice, T.M. Exciton Condensate in Semiconductor Quantum Well Structures. *Phys. Rev. Lett.* **1995** 74, 1633

[9] Ivanov, A.L. Quantum diffusion of dipole-oriented indirect excitons in coupled quantum wells. *Europhys. Lett.* **2002** 59, 586

[10] Schindler, C.; Zimmermann. R. Analysis of the exciton-exciton interaction in semiconductor quantum wells. *Phys. Rev. B* **2008** 78, 045313

[11] Ivanov. A.L.; Muljarov. E.A.; Mouchliadis. L.; Zimmermann. R. Comment on Photoluminescence Ring Formation in Coupled Quantum Wells: Excitonic Versus Ambipolar Diffusion. *Phys. Rev. Lett.* **2010** 104, 179701

[12] Remeika, M.; Graves, J.C.; Hammack, A.T.; Meyertholen, A.D.; Fogler, M.M.; Butov, L.V.; Hanson, M.; Gossard, A.C. Localization-delocalization transition of indirect excitons in lateral electrostatic lattices. *Phys. Rev. Lett.* **2009**, 102, 186803

[13] Note that the exciton density can be also roughly estimated from the light absorption: $n \sim \frac{P_{ex}}{E_{ex} A_{ex}} \alpha\tau$, where P_{ex} is the power of the excitation laser, E_{ex} is the photon energy of the excitation laser, A_{ex} is the excitation spot area, α is the fraction of photons emitted by the excitation laser that is transformed to indirect excitons due to the light absorption and carrier relaxation, and τ is the lifetime of indirect excitons. The uncertainty in the value of α makes such estimate rough. For $\alpha \sim 10^{-2}$, $P_{ex} \sim 2$ μW, $E_{ex} \sim 2$ eV, $A_{ex} \sim 10$ μm^2, and $\tau \sim 50$ ns, the estimate from the light absorption gives $n \sim 3 \times 10^{10}$ cm^{-2} and $N \sim 3 \times 10^3$.